Transient coherent nonlinear spectroscopy of single quantum dots

Wolfgang Langbein and Brian Patton

School of Physics and Astronomy, Cardiff University, Cardiff CF24 3AA, UK

E-mail: LangbeinWW@Cardiff.ac.uk

Abstract

We review our recent advances in four-wave mixing spectroscopy of single semiconductor quantum dots using heterodyne spectral interferometry, a novel implementation of transient nonlinear spectroscopy allowing the study of the transient nonlinear polarization emitted from individual electronic transitions in both amplitude and phase. We present experiments on individual excitonic transitions localized in monolayer islands of GaAs/AlAs quantum wells and in self-assembled CdTe/ZnTe quantum dots. We investigate the formation of the photon echo from individual transitions, both with increasing number of transitions in the ensemble, and in the presence of temporal jitter of the energy of a single transition. The detection of amplitude and phase of the signal allows the implementation of a two-dimensional femtosecond spectroscopy, in which mutual coherent coupling of single quantum dot states can observed and quantified.

(Some figures in this article are in colour only in the electronic version)

1. Introduction

Nonlinear optical spectroscopy is a powerful technique to investigate the electronic structure and dynamics of matter. Specifically, the third-order nonlinearity probed in four-wave mixing (FWM), spectral hole-burning, and pump–probe experiments can be used to determine homogeneous lineshapes of inhomogeneously broadened transitions. Multidimensional nonlinear optical spectroscopy [1] can be used to probe lattice anharmonicities [2] or dynamic pathways of electron–hole excitations [3]. Up to now, these investigations have been limited to studies of large ensembles of the quantum systems under investigation, due to reasons of both signal strength and directional selectivity. With the introduction of the heterodyne spectral interferometry (HSI) technique, we have been able to perform transient four-wave mixing (FWM) measurements on individual, localized excitons. Using a multichannel heterodyne detection, the frequency-resolved third-order polarization is measured in amplitude and phase,

so that both the time-resolved and the spectrally resolved third-order polarization can be retrieved. This enabled us to investigate various nonlinear optical phenomena previously not amenable to study. These include (i) the evolution of the nonlinear response from the case of a free polarization decay to that of a photon echo as the number of individual transitions in an inhomogeneously broadened ensemble is increased; (ii) the separation of homogeneous and inhomogeneous broadening of a single transition; and (iii) the quantification of coherent coupling between excitonic transitions using two-dimensional spectroscopy. The paper is organized as follows: in section 1 we discuss in detail the experimental HSI technique, in section 2 we present the investigated samples, section 3 compares the photoluminescence with the FWM response, section 4 discusses the formation of the photon echo for a small ensemble of states and for a single state with temporal fluctuations, and section 5 is devoted to the two-dimensional FWM enabling the determination of coherent coupling between states.

2. Heterodyne spectral interferometry

Since the size of localized excitonic states in semiconductors is typically much smaller than the wavelength of the resonant light, the light emitted by the polarization of an individual state propagates in all directions (apart from polarization-induced effects), so that the commonly used directional selection of the four-wave mixing signal and other nonlinear optical signals is not effective. To discriminate these signals from the excitation light in this case, we can only use the phase coherence of the signal relative to the excitation pulses, which is determined by the form of the nonlinear polarization, for the two-pulse four-wave mixing, for example, $P^{(3)} \propto \mathcal{E}_1^* \mathcal{E}_2 \mathcal{E}_2$, with the excitation electric fields $\mathcal{E}_{1,2}$. In order to be sensitive to the phase of the emitted FWM field, we need to detect the field by its interference with a reference field $\mathcal{E}_r$ of known phase. Such a detection principle was used to measure pump–probe and four-wave mixing in waveguides [4, 5] and in planar InAs quantum dot ensembles [6]. In these investigations, large ensembles of excitonic states ($>10^5$) were studied, for which the FWM was emitted as a photon echo [7] due to the inhomogeneous broadening of the transition energies in the excited ensemble. Conversely, when probing individual localized transitions, the signal from each transition is expected to be emitted as a free polarization decay, with a linewidth given by the intrinsic dephasing time of the transition, typically several orders of magnitude narrower than the inhomogeneous broadening of the ensemble. The resulting signal from several transitions will therefore be of significant spectral complexity, which requires a multichannel detection if all its components are to be measured simultaneously. Due to the weak signal from individual transitions, only a simultaneous detection of all components provides sufficient sensitivity to allow for experimental feasibility. We have therefore developed a multichannel heterodyne scheme using spectrally resolved detection with a charge-coupled device (CCD), and we retrieve the coherent signal by spectral interferometry [8, 9]. This scheme provides a simultaneous measurement of all spectral components of the signal in both amplitude and phase, allowing the determination of the signal in both the frequency-domain and the time-domain, which are connected by Fourier transformation. We call the resulting spectroscopic implementation of transient nonlinear microscopy heterodyne spectral interferometry (HSI). Conceptually it represents a combination of the previously used phase-stabilized two-dimensional femtosecond spectroscopy [10] and phase-sensitive selection of the nonlinear signal used in heterodyne-detected four-wave mixing [5] or in phase-cycling detection [11].

We now discuss in more detail the implemented two-beam experiment [12]. We use the excitation electric field pulses $\mathcal{E}_{1,2}(t)$ centred at $t = 0$ which have a relative delay time τ, so that $\mathcal{E}(t) = \mathcal{E}_1(t + \tau) + \mathcal{E}_2(t)$. A generalization of the experiment to more pulses does

not involve any qualitative changes of the scheme. The polarization response function R of a medium can be developed into different orders $R^{(n)}(\tau, t)$ in the excitation field $\mathcal{E}(t)$ [13]. Each $R^{(n)}$ is a sum of contributions of different order in the fields $\mathcal{E}_{1,2}$, i.e. $R^{(\mathbf{n})} \propto \mathcal{E}_1^{n_1} \bar{\mathcal{E}}_1^{m_1} \mathcal{E}_2^{n_2} \bar{\mathcal{E}}_2^{m_2}$ with $\mathbf{n} = (n_1, m_1, n_2, m_2)$ and $n = n_1 + m_1 + n_2 + m_2$, where the exponents $n_{1,2}$ and $m_{1,2}$ are natural numbers including zero. In extended media, one can discriminate the orders experimentally using defined wavevectors of the excitation fields $\mathbf{k}_{1,2}$, in which case the polarization $R^{(\mathbf{n})}$ emits in the direction $l_1 \mathbf{k}_1 + l_2 \mathbf{k}_2$ with $l_1 = n_1 - m_1$ and $l_2 = n_2 - m_2$. For sub-wavelength-sized media, like individual excitonic transitions, the broken translational invariance prohibits the use of such a wavevector selection. However, we can still use the time invariance[1] of the response function to select $R^{(\mathbf{n})}$ by repeating the experiment with controlled variations in the phases of the pulses $\mathcal{E}_{1,2} \propto e^{i\varphi_{1,2}}$. In the limit of a large number of repetitions, the time-ensemble averaged response function is measured in this way. To measure repeats that are independent of each other, the repetition period τ_p has to be longer than the memory time of the response function, which is typically given by the dephasing times and density lifetimes of the resonant transitions in the medium. The different orders of the response function are then discriminated by their Fourier transform versus $\varphi_{1,2}$:

$$R_s^{l_1, l_2} = \int R(\varphi_1, \varphi_2) e^{(-il_1\varphi_1 - il_2\varphi_2)} \, d\varphi_1 \, d\varphi_2. \tag{1}$$

The selected $R_s^{l_1, l_2}$ is the sum over all $R^{(\mathbf{n})}$ with equal l_1, l_2. The individual components $R^{(\mathbf{n})}$ are of different orders in $|\mathcal{E}_{1,2}|$, and they can be distinguished by their dependences on the field amplitudes. For example, the FWM showing a photon echo for positive τ corresponds to $\mathbf{n} = (0, 1, 2, 0)$, so that $l_1 = -1$ and $l_2 = 2$, i.e. it scales linearly with $|\mathcal{E}_1|$ and quadratically with $|\mathcal{E}_2|$. If we use excitation pulses of equal carrier frequency, the response field at this carrier frequency is given by contributions with $|l_1 + l_2| = 1$, as is the case for the linear response and the photon echo.

A schematic diagram of the experimental setup used for the experimental results presented here is given in figure 1. Optical pulses of about 150 fs duration at a repetition rate of $2\pi/\tau_p = \Omega_p = 2\pi \times 76$ MHz were produced by a mode-locked Ti:sapphire laser. The pulses were spectrally shaped to resonantly excite the selected ensemble of localized exciton states. The pulses were split into two beams $P_{1,2}$ that were subsequently phase and frequency shifted with acousto-optical modulators (AOMs) by $\varphi_{1,2} = \Omega_{1,2}t$ with $\Omega_{1,2} = 2\pi \times (79, 80)$ MHz. They were then recombined in a beam-splitter cube into the same spatial mode P_s, with a relative delay time τ, positive for pulse 1 leading. A reference beam P_r (the part of P_2 not deflected by the AOM) propagates close to P_s and fills, as with P_s, the far-field plane (FF) of the microscope objective (MO). By passing through the same optical elements after the beam-splitter cube, phase fluctuations between P_r and P_s are minimized. The path over which the beams travel separately is encapsulated, minimizing phase fluctuations due to air turbulence. The whole setup is temperature stabilized. The beams are coupled into the MO using a beam splitter of only 4% reflectivity in order to reduce the losses in the subsequent transmission in the detection path. The beams are focused onto the sample plane, called the near-field plane (NF), by an achromatic MO of 0.85 numerical aperture. This MO was mounted in the cryostat sample chamber on a piezoelectric translation stage, allowing for fine positioning of the focus with 10 nm sensitivity. The response field emitted in the reflected direction is collected by the same MO and spatially filtered at an intermediate image plane to keep only the zeroth order of the Airy diffraction created by the objective aperture for both P_r and P_s (see the NF image in figure 1). From there, a dual lens system (L2, L3) images the FF into a mixing AOM, in which P_r and P_s spatially overlap. The NF is instead imaged into the directions at the AOM,

---

[1] This demands a temporal stability of the investigated structure over the course of the experiment.
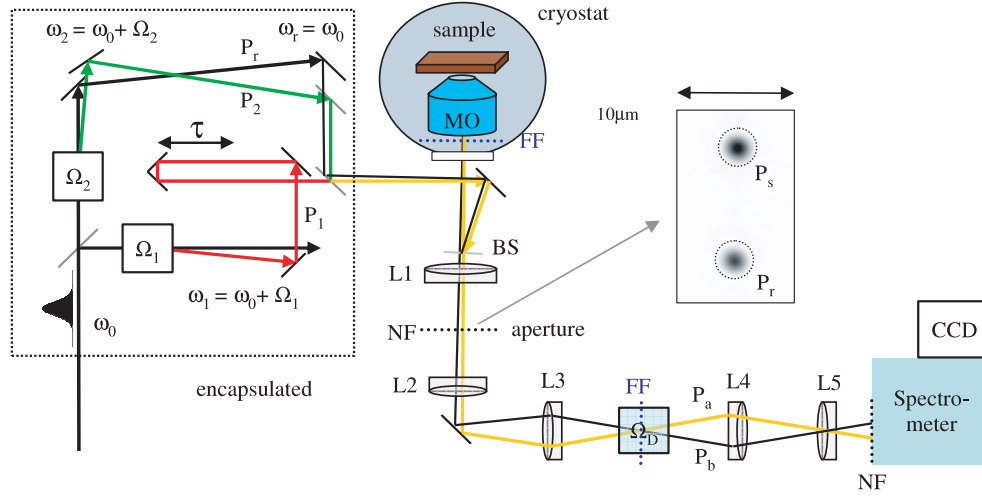
Figure 1. Scheme of the experimental setup. Boxes: acousto-optical modulators of the indicated frequency. MO: high numerical aperture (0.85) microscope objective, L1–L5 achromatic doublet lenses. Spectrometer: imaging spectrometer of 15 μeV resolution. NF: near field of sample, FF: far field of sample.

so that the spatial separation between P_r and P_s in the NF ($\approx 9\ \mu$m) corresponds to different directions in the AOM. The angle between these directions is chosen to match the AOM Bragg diffraction angle (0.015 rad). By this arrangement, the diffracted beam of P_r overlaps with P_s and vice versa. The resulting mixed beams $P_{a,b}$ pass through a dual lens system (L4, L5) that images the NF into the input slit of a high-resolution (15 μeV) imaging spectrometer where $P_{a,b}$ are spatially separated, while the FF is imaged onto the spectrometer grating to avoid vignetting. The spectrally resolved and time-resolved intensities $I_{a,b}(\omega, T)$ of $P_{a,b}$ are detected by a liquid nitrogen cooled silicon charge-coupled device (CCD) at the output focus plane of the spectrometer. In this notation ω denotes the optical frequencies, with a resolution limited by the spectrometer (≈ 3 GHz), while T denotes the lower-frequency time dynamics, which parameterizes the repeated measurements with different $\varphi_{1,2}$.

The mixing AOM is driven with an electric field $\propto \cos(\Omega_D T + \varphi)$, so that P_s acquires a phase shift $-\Omega_D T - \varphi$ when diffracted into P_r, while P_r is phase-shifted by $\Omega_D t + \varphi$ when diffracted into P_s. The diffraction efficiency is adjusted to 50%, so that the detected intensities are $2I_{a,b}(\omega, T) = |\mathcal{E}_r|^2 + |\mathcal{E}_s|^2 \pm 2\,\mathrm{Re}(\mathcal{E}_r\bar{\mathcal{E}}_s e^{i\Omega_D T + \varphi})$ with the reference and signal fields $\mathcal{E}_{r,s}$. We detect $I_{a,b}(\omega, T)$ integrated over the CCD exposure time $T_e \approx 50$–1000 ms. To extract the interference term only, we determine $I_d(\omega) = I_a - I_b = 2 \int_0^{T_e} \mathrm{Re}(\mathcal{E}_r\bar{\mathcal{E}}_s e^{i\Omega_D T + \varphi})\mathrm{d}T$. In this quantity, the time-integration results in a low-pass filter $\sin(x)/x$ with $x = T_e\Omega/2$, suppressing frequencies $\Omega > 4/T_e$. The response $R_s^{l_1, l_2}$ has the interference frequency $\Omega_i = l_1\Omega_1 + l_2\Omega_2 - \Omega_D$. Since $\mathcal{E}_r$ is much shorter than the repetition period, $\mathcal{E}_r e^{i\Omega_D}$ contains many sidebands separated by Ω_p, and Ω_i is thus only defined modulo Ω_p. By the choice of Ω_1, Ω_2 and Ω_p, the Ω_i corresponding to different $l_{1,2}$ are differing in the megahertz range. To select $R_s^{l_1, l_2}$ in I_d, we use $\Omega_D = l_1\Omega_1 + l_2\Omega_2$ to shift Ω_i to zero, so that $R_s^{l_1, l_2}$ is not suppressed, while other $R_s^{l'_1, l'_2}$ are suppressed by factors of $T_e\Omega'_i > 10^6$. In order to avoid the background due to systematic variations of detection efficiencies in $I_{a,b}(\omega)$, for example due to inhomogeneities in the CCD response, φ is cycled by π between adjacent exposures, and we use $2I_d = I_d^{\varphi=0} - I_d^{\varphi=\pi}$. In this way, the classical noise and systematic errors from the

non-interfering term $|\mathcal{E}_r|^2 + |\mathcal{E}_s|^2$ are largely suppressed, and the weak interference signal can be detected in shot-noise limited conditions. Note that $\mathcal{E}_s$ also contains the linear reflection of $\mathcal{E}(t)$, which typically by far dominates its intensity, and that $|\mathcal{E}_r|^2$ has to be significantly larger than $|\mathcal{E}_s|^2$ to reach shot-noise limited detection. This results in a weak interference due to $R_s^{l_1,l_2}(\omega)$, typically below 10^{-3} relative modulation, which can only be detected in a well-balanced scheme.

$R_s^{l_1,l_2}(\omega)$ is determined from I_d by spectral interferometry [9], using the experimentally adjusted property of $\mathcal{E}_r$ to precede the signal field in time t. Using this property, we can apply $F(\Theta(t)F^{-1}(I_d(\omega))) = \mathcal{E}_r^*(\omega)R_s^{l_1,l_2}(\omega)$ with the Heaviside function $\Theta(t)$, and the Fourier-transform operator F. The reference field amplitude can be determined by blocking P_s and measuring $I_{a,b} = |\mathcal{E}_r|^2$ in this case. Since $\mathcal{E}_r$ is the reference pulse reflected by the sample it is helpful to arrange that the reflection does not strongly modify its spectrum. This can be achieved by a metal coating on the sample with an opening at the signal beam, or by using a surface reflection that is dominated by a non-resonant refractive index. Different $R_s^{l_1,l_2}$ including their relative phase can be measured sequentially during the passive phase stability time of the setup. In order to correct for long-term drifts of the relative phase between the signal and reference within a measurement consisting of many CCD exposures, the phase of the measured signal is determined for subintervals of the total acquisition time. If the nonlinear signal in the subintervals is too weak to determine the phase, one can monitor the phase drifts of $R_s^{1,0} \propto e^{i\varphi_1}$ and $R_s^{0,1} \propto e^{i\varphi_2}$ instead.

In this way, different material responses can be measured sequentially: for $\Omega_d = \Omega_{1,2}$, the reflected excitation pulses 1, 2 are measured, while for $\Omega_d = 2\Omega_2 - \Omega_1$, the emitted FWM field $\propto \mathcal{E}_1^*\mathcal{E}_2^2$ is measured. Higher-order nonlinearities, like six-wave mixing, can be detected analogously.

3. Samples

We have investigated two different sample types with the HSI technique. Samples of type (i) are localized excitons in thin GaAs/AlAs quantum wells grown with a growth interrupt to enable the formation of large monolayer islands [14, 15, 12]. These samples are described in [16], and they were also investigated by time-resolved and spectrally resolved speckle analysis [17, 18]. A detailed theoretical model of the interface structure and the excitonic properties is given in [19]. Samples of type (ii) are self-assembled epitaxial CdTe/ZnTe quantum dots (QDs) [20]. In this review we will concentrate on results on samples of type (i). They consist of an AlAs/GaAs/AlAs single quantum well grown by molecular-beam epitaxy with a thickness increasing from approximately 4 to 10 nm over a total lateral displacement of 200 mm. The growth was interrupted for 120 s at each interface, allowing for the formation of large monolayer islands on the growth surface. The sample was antireflection coated, and was held in a helium cryostat at a temperature of $T = 5$ K.

4. Photoluminescence versus four-wave mixing

For non-resonant excitation at 1.96 eV, spatially focussed to the diffraction limit of the MO, the confocally detected photoluminescence (PL) of an approximately 6 nm thick region of the QW is shown in figure 2(a). In order to select individual states within the optical resolution of the experiment (0.5 μm), we adjusted the fractional monolayer thickness of the QW to be about -0.2 ML, yielding a low density of localized exciton states in the largest monolayer (ML) thickness [19]. Due to the diffusion of the excited carriers prior to recombination, the spatial resolution of the PL spectrum is determined by the resolution of 0.61 λ/NA in the emission imaging. The same region was investigated by the FWM technique. The excitation
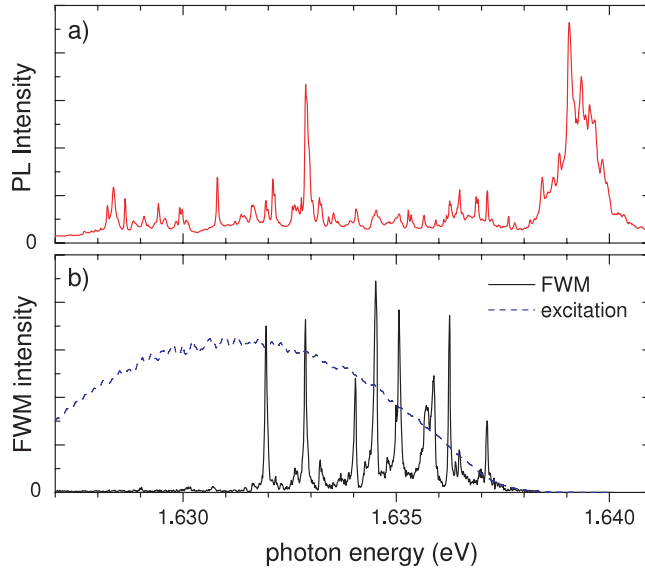
Figure 2. (a) Confocally excited/detected PL spectrum of a $(0.5 \ \mu\text{m})^2$ area of an AlAs/GaAs QW with a thickness of about 20.8 ML (6 nm). (b) Spectrally resolved FWM intensity of the same area at $\tau = 1$ ps. The spectrum of the excitation pulses is shown as a dotted line.

spectrum (see figure 2(b)) was resonant only to excitons localized in the lower monolayer in order to avoid creating large exciton densities. The measured spectrally resolved FWM for a small positive delay time $\tau = 1$ ps is shown in figure 2(b). It consists of several sharp resonances of 20–30 μeV full width at half maximum (FWHM). Since the FWM intensity is proportional to the third power of the excitation intensity (in the low excitation intensity limit), the spatial resolution in the FWM can be improved to $0.36 \ \lambda/\text{NA} \approx 320$ nm. FWM resonances of significant strength are only observed at the higher-energy side of the PL emission, and the FWM intensities of the resonances are not clearly correlated to the PL intensities. This is due to the different properties probed by PL and FWM. The FWM intensity is (in the low excitation intensity limit) proportional to the eighth power of the optical transition dipole moment μ of the resonance. The PL intensity instead is determined by the radiative rate, proportional to μ^2, but also by the relaxation dynamics of excitons into the localized state. Additionally, in the PL we use non-resonant excitation, for which charged exciton emission [21], having a binding energy of about 4 meV, could be present, explaining the PL below 1.630 eV.

Due to the weak signal obtainable from single transitions, measurements are typically performed at excitation intensities at the upper limit of the third-order regime, at which higher-order contributions can be relevant. To illustrate this, we show in figure 3 the dependence of the detected FWM intensity on the excitation intensity. We find that a third-order scaling is only observed for the two smallest intensities used, while at higher intensities the signal saturates. We have used the possibility of strong excitation to perform coherent optical manipulation such as Rabi flopping, as reported in [15].

5. Photon echo formation

For positive delay times τ, the FWM detected at $\Omega_d = 2\Omega_2 - \Omega_1$, which is proportional to the phase-conjugated electric field of the first pulse $\mathcal{E}_1^*$, shows the so-called photon echo,
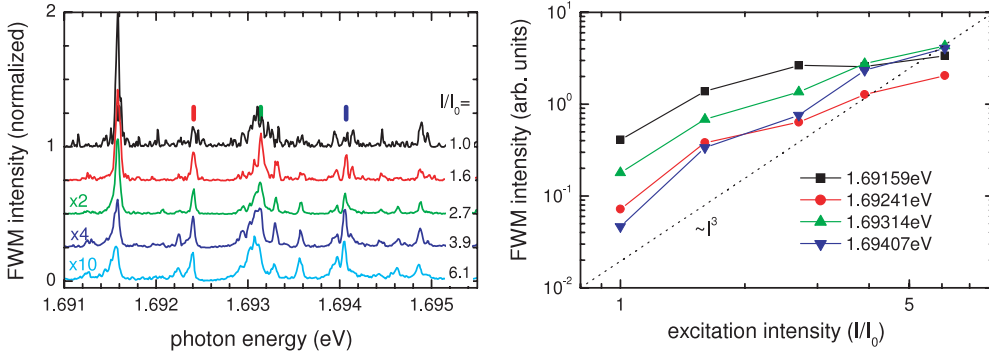
Figure 3. Spectrally resolved FWM intensity of a different sample area compared to figure 2 at $\tau = 0.5$ ps for various excitation intensities I/I_0 as given, with $I_0 = 1.5\ \mu$W. The excitation and detection polarizations were linear $(\rightarrow, \rightarrow, \rightarrow)$. In the left plot, the data have been normalized by the third-order behaviour I^3; they are vertically offset for clarity, and are magnified by the factors indicated. In the right plot, the intensity of various FWM peaks (indicated in the left plot with bars) is shown as a function of the excitation intensity. A third-order scaling $\propto (I/I_0)^3$ is shown for comparison (dotted line).
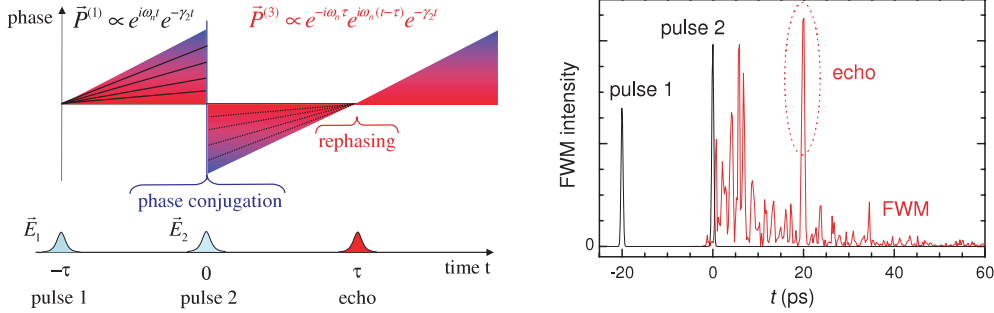

Figure 4. Left: scheme of the echo formation in transient FWM. Right: measured time-resolved FWM intensity from a group of exciton states localized within an $(0.5\ \mu$m$)^2$ area. Excitation pulses 1, 2 (black) and time-resolved FWM intensity (red, oscillating line) for a delay time of $\tau = 20$ ps are shown.

which is a well-known feature and has been observed first in spin echoes [22], and later also in the optical frequency range [23]. Due to the specific nonlinearity probed at this frequency, the FWM phase at a time τ after the arrival of the second pulse does not depend on the eigenfrequency of the two-level system, and thus a macroscopic polarization is created even in presence of an ensemble of transitions with different transition energies (inhomogeneous broadening). This mechanism is illustrated in the left part of figure 4. In a representative measurement, shown in the right part, the formation of the echo in a finite ensemble is observed as intensity enhancement at the time of the echo. Here and in the following we have fixed the time-zero to the arrival of the second pulse; thus the first pulse arrives at $t = -\tau$, and the echo is created at $t = \tau$.

Generally, we can write the FWM polarization for $\tau > 0$ and $t > 0$ for a set of N two-level systems with transition frequencies $\tilde{\omega}_k$ as

$$R^{(0,1,2,0)}(t,\tau) = \sum_{k=1}^{N} \mu_k^4 |\mathcal{E}_1(\tilde{\omega}_k)\mathcal{E}_2^2(\tilde{\omega}_k)| e^{i\tilde{\omega}_k(t-\tau)-\gamma_k(t+\tau)} \qquad (2)$$

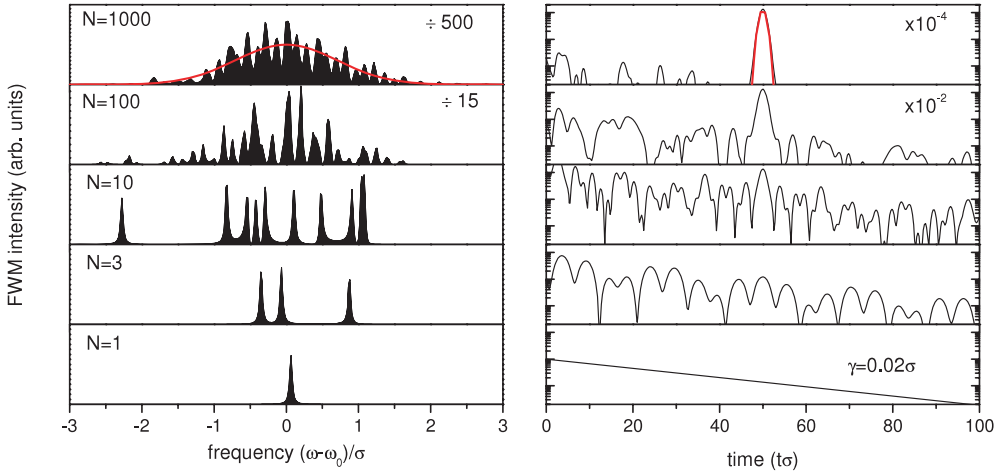with the dipole moments of the transitions μ_k and the appropriately normalized excitation field

Figure 5. Simulated spectrally resolved FWM intensity (left) and time-resolved FWM intensity (right) for ensembles of N two-level systems with equal transition dipole moment μ and dephasing rate $\gamma = 0.02\,\sigma$, but transition frequencies ω_k taken from a Gaussian distributed ensemble of variance σ (indicated as a red line in the $N = 1000$ FWM spectrum, together with corresponding the FWM echo in the FWM dynamics).

amplitudes $\mathcal{E}_{1,2}(\omega)$ of pulse 1, 2 at the frequency ω. By taking the resonant field amplitudes in this equation, we assume that the spectral width of the excitation pulse is much larger than the dephasing rates γ_k of the transitions. At $t = \tau$, the FWM fields from all two-level systems are in phase, and therefore interfere constructively. This results in a signal amplitude N times larger than the individual FWM amplitudes of a single transition. For other times, the phases are, in general, randomly distributed due to the distribution of the transition frequencies, and the signal amplitude is only about $\sqrt{N}$ times the individual amplitude. In the limit of a large number of systems in the ensemble, the signal at $t = \tau$ is thus far larger than at other times, and is called a photon echo.

A simulation of the formation of the photon echo with increasing size N of the ensemble is given in figure 5. The transition energies were chosen from a Gaussian distribution of variance σ. While for a single transition the FWM dynamics is a free polarization decay, the presence of several transitions leads to pronounced interference oscillations in the signal, which show constructive interference at the photon echo time. With increasing N, this constructive interference develops into a Gaussian photon echo dominating the response. For $N = 1000$, the response is already close to the limit $N \to \infty$, which is given as red lines for comparison. We can compare this simulation with our experimental results by appropriate selection of regions of the sample, to control the size of the state ensemble probed in the FWM. By systematically increasing the number of participating transitions from one to many, we can follow the formation of the photon echo with increasing ensemble sizes. This evolution is shown in figure 6 for ensembles of about 1, 4, and 10 transitions. With increasing ensemble size N, the intensity enhancement in the photon echo increases roughly $\propto N$, as expected from equation (2).

Apart from the evolution from a free polarization decay to a photon echo by increasing the number of individual transitions in the ensemble, we find that even individual transitions can show a photon echo in the FWM when measured by the HSI technique. This is due to the fact that measurements on single transitions need a large number of repetitions, as the signal
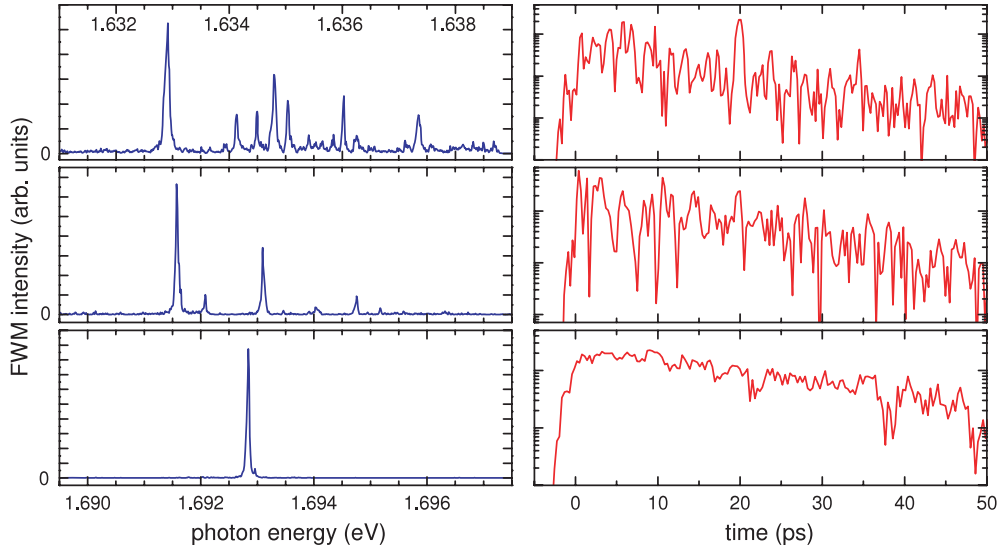
Figure 6. Measured FWM intensity for $\tau = 20$ ps, spectrally resolved (left) and time resolved (right), for exciton state ensembles of different size.

created in an individual measurement is small: at maximum one can detect a single photon in a single measurement, but typically on average only $10^{-2} \ldots 10^{-5}$ photons are detected due to the limited collection efficiencies, detection efficiencies, and also to less than one photon initially being emitted. In the measurements presented here, we average over 1–100 s for each FWM spectrum, corresponding to $10^{10} \ldots 10^{12}$ repetitions. During this time, slow fluctuations of the environment of the probed transition can lead to a variation of its frequency (e.g. by the Stark effect due to local electric field variations), resulting in an effective inhomogeneous broadening in the time-ensemble probed by the measurement [1]. This manifests itself by a typical linewidth of individual excitonic transitions in semiconductor quantum dots at low temperatures measured in the single-dot photoluminescence of 100–1000 μeV [24–27], much larger than their homogeneous linewidth as determined in large-ensemble photon echo experiments in the 1–10 μeV range [28, 7]. Since the HSI measures the time-ensemble average of the FWM *field*, this effective inhomogeneous broadening also leads to the formation of a photon echo. In the GaAs/AlAs samples only weak spectral wandering is observed, leading to a temporally wide echo, similar or wider than the dephasing time. Much stronger spectral wandering was observed in measurements on CdTe quantum dots (sample type (ii)) [20].

The spectral FWM intensity from a region of sample type (ii) with exciton states of significant linewidth is given in the inset of figure 7, showing a lineshape of about 0.35 meV FWHM. To investigate the time-evolution of the FWM from the single transition, we spectrally filter the FWM around the transition (see inset) with a Gaussian of 0.62 meV FWHM. The resulting time-evolution of the FWM intensity is given in figure 7 for various delay times. A shift of the FWM with increasing delay time is observed. The transition thus does show a photon echo as opposed to a free polarization decay, indicating that it is dominantly inhomogeneously broadened. The homogeneous broadening of the transition is given by the photon echo intensity at $t = \tau$, decaying with τ like $\propto \exp(-4\tau/T_2)$. This analysis yields $T_2 = 20 \pm 5$ ps, corresponding to a homogeneous linewidth of $2/T_2 = 66$ μeV FWHM, significantly smaller that the total linewidth measured.
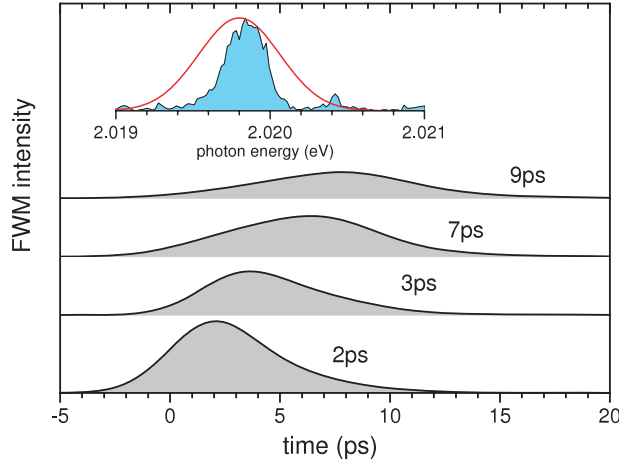
Figure 7. Time-resolved FWM from a single excitonic transition in a CdTe/ZnTe quantum dot at various delays τ. The inset shows the spectrally resolved FWM intensity at $\tau = 7$ ps, and the filter function used to isolate the single transition (red solid line).

6. Two-dimensional spectroscopy

Multidimensional nonlinear optical spectroscopy [1] is an analogue of multidimensional nuclear magnetic resonance, which enables one to determine the coherent coupling between the resonances present in the system. Up to now, these investigations have been limited to studies of large ensembles of the quantum systems under investigation, due to reasons of both signal strength and directional selectivity. With the HSI technique, this multidimensional technique has become feasible also for individual excitonic states [12, 20].

In figure 8(a) we show delay-time-dependent FWM spectra $|R_s^{-1,2}(\tau, \omega)|^2$ for a localized exciton system in a sample of type (i). The strong intensity modulation versus delay time (also called quantum beats) of some peaks indicate the presence of a coherent coupling between them, where the beat period is given by the frequency difference of the coupled first-order resonances. The coherent coupling between excitonic states is of specific interest for their application in quantum computation. The most common coupling mechanisms are Coulomb interaction, exchange interaction, and coupling via the near-field of the optical polarization (Förster coupling). Since we know the signal in amplitude and phase for each measured delay time τ, we can not only look at the intensity beating, which is non-straightforward to interpret, but we can also Fourier transform the delay-time dependence of the signal for $\tau > 0$, resulting in the conjugated frequency variable ω_1. This procedure yields the two-dimensional frequency domain data $|R_s^{-1,2}(\omega_1, \omega)|^2$ (see figure 8(b)). For $\tau > 0$ the FWM signal is proportional to the first-order polarization created by the first pulse, probed at the arrival time of the second pulse. Since this polarization is freely evolving in the transitions of the system during the time interval τ, the frequency variable ω_1 gives the first-order frequency of the transition creating the FWM signal. Fourier transforming the data for negative delay times $\tau < 0$ instead results in the frequency variable ω_2, which is given by the frequency of the two-photon coherences, which are propagating freely in the time between their creation by the second pulse and the transformation into the FWM signal by the first pulse, as we will discuss in a forthcoming work. We can see in $|R_s^{-1,2}(\omega_1, \omega)|^2$ that each third-order resonance (i.e. in ω) is created by one or more first-order resonances (in ω_1). For uncoupled two-level systems, only one transition frequency exists in each system, so that the first-order and third-order resonance frequencies
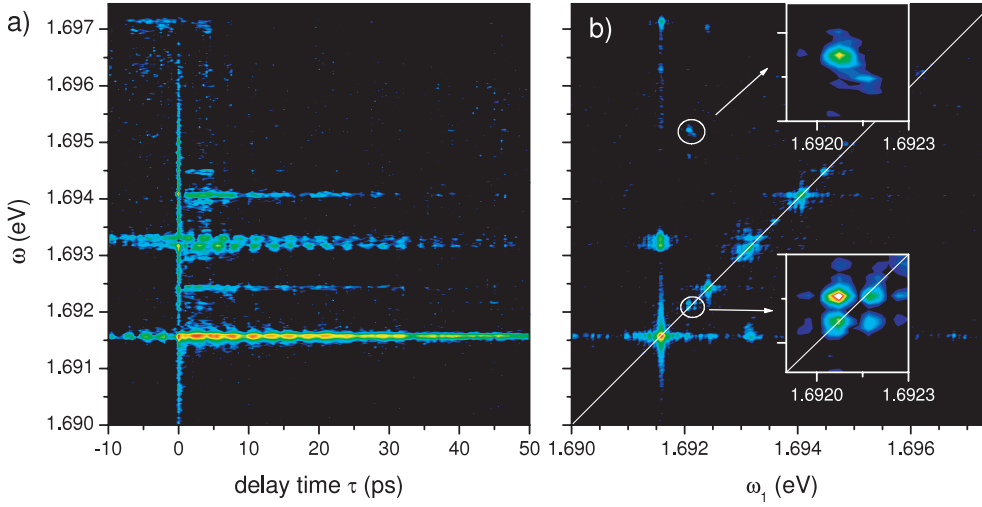
10

Figure 8. Two-dimensional FWM of the same sample region as figure 3. Co-circular excitation polarizations were used for pump, probe, and detection ($\sigma^+\sigma^+\sigma^+$). (a) $|R_s^{-1,2}(\tau,\omega)|^2$ on a logarithmic colour (grey) scale over 2 orders of magnitude for delay times $\tau = -10\ldots 50$ ps. (b) $|R_s^{-1,2}(\omega_1,\omega)|^2$ calculated from (a) for $\tau > 0$ on a logarithmic colour (grey) scale over 3.5 orders of magnitude. The insets show magnifications of a fine-structure split exciton and the coupled unbound biexciton.

are equal, and the related FWM signal in $|R_s^{-1,2}(\omega_1,\omega)|^2$ is on the diagonal $\omega_1 = \omega$. We find that the measured data are actually dominated by such diagonal resonances. However, off-diagonal peaks are also present, giving evidence for the presence of coherent coupling between the corresponding exciton states [13]. In the third-order regime, the off-diagonal peaks of two first-order resonances on both sides of the diagonal are expected to be equal in intensity, while in the experimental data the intensities are observed to be somewhat different, stronger for $\omega_1 < \omega$. This could be related to higher-order contributions, as preliminary simulations have shown [29]. The spectra corresponding to individual first-order frequencies are given in figure 9, together with a spectrum of the diagonal response $\omega_1 = \omega$.

The simplest case showing coupling is the coherent coupling of two excitons. Such a coupling could be diagonalized, resulting in a four-level excitonic system consisting of the new excitonic eigenstates including the interaction [30]. A prominent example would be the exciton–biexciton system in the lowest excitonic state of a quantum dot. There, the two spin-degenerate exciton eigenstates are coupled by the long-range exchange interaction, resulting in two linearly polarized excitonic states, and the Coulomb interaction and correlation between the two excitons leads to an energy renormalization of the biexciton state. In such a system, the resonances in ω of the two-dimensional response $R_s^{-1,2}(\omega_1,\omega)$ can be different from ω_1. The resonances in ω_1 would be the two fine-structure split excitons, and for each of these resonances we would detect resonances in ω given by all four transitions in the four-level system, i.e. the two excitonic and the two biexcitonic transitions.

Generally, in a multilevel system with transition frequencies $\tilde{\omega}_k$ and dipole moments μ_k, the third-order response for positive delay times (neglecting damping for simplicity) can be written as

$$R^{(0,1,2,0)}(t > 0, \tau > 0) \propto \sum_{k \in X} \mu_k e^{-i\tilde{\omega}_k \tau}\left(\sum_l \mu_l A_{kl} e^{i\tilde{\omega}_l t}\right) \tag{3}$$
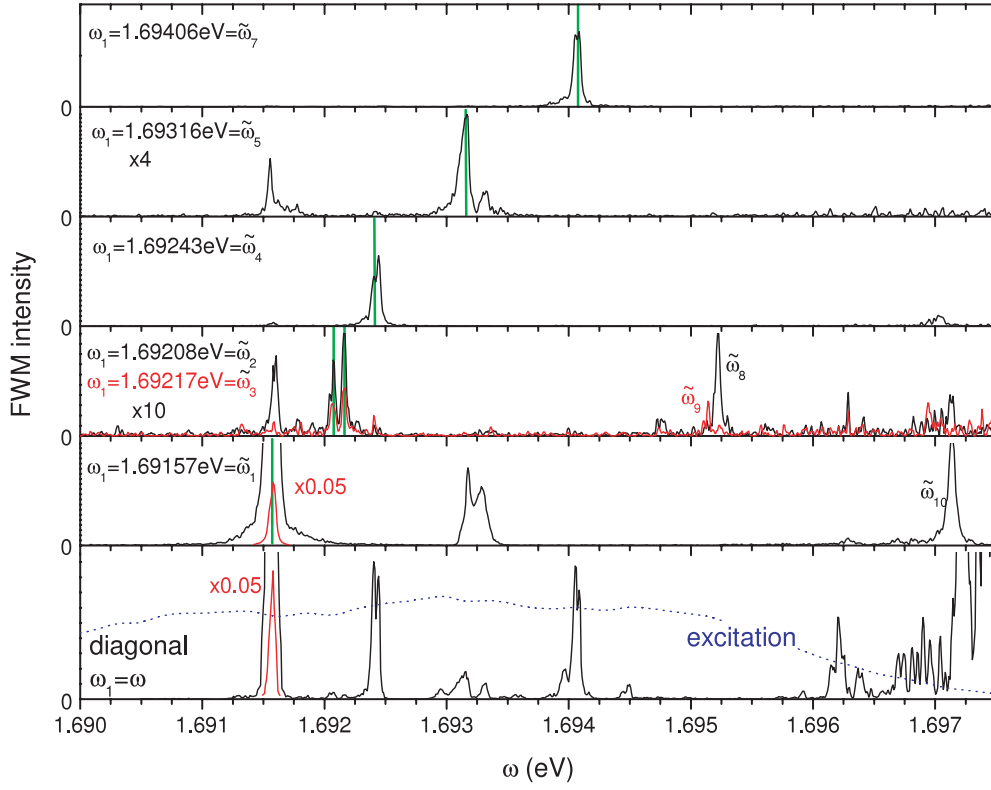
Figure 9. Spectra taken from the two-dimensional FWM of figure 8(b), corrected for the excitation pulse spectrum $|\mathcal{E}(\omega)|^2$. In the lowest frame the diagonal intensity $|R_s^{-1,2}(\omega,\omega)|^2/|\mathcal{E}(\omega)|^6$ is given, while in the other frames $|R_s^{-1,2}(\omega_1,\omega)|^2/|\mathcal{E}(\omega)|^2$ are given for selected $\omega_1 = \tilde{\omega}_k$ as indicated. The relative data scaling factors are shown.

where A_{kl} describes the polarization transfer from the transition k (first-order resonance) to the transition l (third-order resonance) by the second excitation field. X denotes the excitonic transitions i.e. from the crystal ground state (the initial state in the experiment) to a single electron–hole pair. These are the only ones excitable in first order. Infinitely short excitation pulses are assumed here, which have a spectrally flat amplitude. Fourier transforming $t \to \omega$ and $\tau \to \omega_1$ gives

$$R^{(0,1,2,0)}(\omega,\omega_1) \propto \sum_{k \in X} \mu_k \delta(\omega_1 + \tilde{\omega}_k) \left(\sum_l \mu_l A_{kl} \delta(\omega - \tilde{\omega}_l) \right). \tag{4}$$

For uncoupled two-level systems we have $A_{kl} = \delta_{kl}\mu_k\mu_l$, so that only peaks along $\omega_1 = \omega$ are present. The spectral width of the peaks in the experiment is determined by the respective dephasing of the observed transition. Coupled transitions $k \neq l$ instead create diagonal and off-diagonal peaks at $(\omega,\omega_1) = (\tilde{\omega}_l, \tilde{\omega}_k)$, where the amplitudes would still be given by $A_{kl} = \mu_k\mu_l$, provided that the coupling energy is larger than the linewidth.

After these general remarks on the structure of the two-dimensional spectra, we now discuss details of the interpretation of the measurement presented in figure 8(b). We observe that the dominating peak at $\tilde{\omega}_1 = 1.69156$ eV is coupled to the first-order resonance doublet $\tilde{\omega}_{4,5}$ around 1.6932 eV, split by 0.1 meV, and separated by 1.6 meV to $\tilde{\omega}_1$. This coupling is the origin of the strong quantum beats in the intensities of $\tilde{\omega}_{1,4,5}$ versus τ. Knowing the

12

typical structure of the confined excitonic states [19], the transition $\tilde{\omega}_1$ could be an exciton in the lowest confined state of a large monolayer island, which shows no significant fine-structure splitting but a strong transition dipole moment, leading to the observed strong FWM signal. The transitions $\tilde{\omega}_{4,5}$ could then be higher exciton states in the same monolayer island, showing a small splitting due to the lifting of the in-plane degeneracy of the p-states, and a factor of about 1.8 smaller transition dipole moment (taken from the FWM intensity ratio of about 100), comparable to the simulations in figures (16)–(19) in [19]. In the spectrum for $\omega_1 = \tilde{\omega}_1$ (see figure 9), not only are the coupled transitions $\tilde{\omega}_{4,5}$ present, but also another one at $\tilde{\omega}_{10} = 1.69714$ eV. The diagonal response at $\tilde{\omega}_{10}$ is weak since the excitation spectral intensity is reduced significantly, so that the corrected data are too noisy to decide if $\tilde{\omega}_{10}$ is a an exciton transition ($\in X$) or an exciton–biexciton transition.

A clearer picture is found for the $\tilde{\omega}_{2,3}$ doublet, having a splitting of 0.1 meV. It is present on the diagonal, so it represents exciton transitions. It is coherently coupled within itself, and $\tilde{\omega}_2$ is additionally coherently coupled to $\tilde{\omega}_9$, and $\tilde{\omega}_2$ with $\tilde{\omega}_8$. The transitions $\tilde{\omega}_{8,9}$ are not visible on the diagonal, i.e. they are exciton–biexciton transitions (see also insets in figure 8(b)). Observing that $\tilde{\omega}_2 + \tilde{\omega}_9 = \tilde{\omega}_3 + \tilde{\omega}_8$, this set of transitions can be attributed to an exciton–biexciton system consisting of a fine-structure split exciton pair $\tilde{\omega}_{2,3}$ with the transitions $\tilde{\omega}_{9,8}$ to a unsplit biexciton state of negative binding energy of 3.1 meV.

The transitions $\tilde{\omega}_4$ and $\tilde{\omega}_7$ do not show strong coherently coupled transitions within the probed energy range, but both show a weak splitting of some 30 μeV. They are likely excitons localized in slightly anisotropic monolayer islands, leading to a small fine-structure splitting. The island size is probably smaller than for $\tilde{\omega}_1$, reducing the transition dipole moment and shifting the second confined states further way in energy, out of the range of the excitation pulses. For $\tilde{\omega}_4$ the weak peak at 1.697 eV could be due to such an excited state.

As we have seen, there is a wealth of information contained in a single two-dimensional FWM measurement, and we are just at the beginning of its correct interpretation. The lineshape of the peaks including their relative phase will provide for a distinction between different coupling processes, and the linewidths measure the dephasing rates of the transitions. By analysing the negative delay time dynamics, the properties of the two-photon coherences (i.e. ground state to biexciton) can also be measured [31].

Acknowledgments

References

[1] Mukamel S 1999 *Principles of Nonlinear Optical Spectroscopy* (USA: Oxford)
[2] Khalil M, Demirdöven N and Tokmakoff A 2003 *Phys. Rev. Lett.* **90** 047401
[3] Brixner T, Stenger J, Vaswani H M, Cho M, Blankenship R E and Fleming G R 2005 *Nature* **434** 625
[4] Hall K L, Lenz G, Ippen E P and Raybon G 1992 *Opt. Lett.* **17** 874
[5] Borri P, Scaffetti S, Mørk J, Langbein W, Hvam J M, Mecozzi A and Martelli F 1999 *Opt. Commun.* **164** 51
[6] Langbein W, Borri P, Woggon U, Stavarache V, Reuter D and Wieck A D 2004 *Phys. Rev.* B **70** 033301
[7] Borri P, Langbein W, Schneider S, Woggon U, Sellin R L, Ouyang D and Bimberg D 2001 *Phys. Rev. Lett.* **87** 157401
[8] Emde M F, de Boeij W P, Pshenichnikov M S and Wiersma D A 1997 *Opt. Lett.* **22** 1338
[9] Lepetit L, Chériaux G and Joffre M 1995 *J. Opt. Soc. Am.* B **12** 2467

[10] Brixner T, Stiopkin I V and Fleming G R 2004 *Opt. Lett.* **29** 884
[11] Tian P, Keusters D, Suzaki Y and Warren W S 2003 *Science* **300** 1553
[12] Langbein W and Patton B 2006 *Opt. Lett.* **31** 1151
[13] Mukamel S 2000 *Annu. Rev. Phys. Chem.* **51** 691
[14] Langbein W and Patton B 2005 *Phys. Rev. Lett.* **95** 017403
[15] Patton B, Woggon U and Langbein W 2005 *Phys. Rev. Lett.* **95** 266401
[16] Leosson K, Jensen J R, Langbein W and Hvam J M 2000 *Phys. Rev.* B **61** 10322
[17] Langbein W, Leosson K, Jensen J R, Hvam J M and Zimmermann R 2000 *Phys. Rev.* B **61** R10555
[18] Kocherscheidt G, Langbein W and Savona V 2003 *Phys. Status Solidi* b **238** 486
[19] Savona V and Langbein W 2006 *Phys. Rev.* B **74** 75311
[20] Patton B, Langbein W, Woggon U, Maingault L and Mariette H 2006 *Phys. Rev.* B **73** 235354
[21] Tischler J G, Bracker A S, Gammon D and Park D 2002 *Phys. Rev.* B **66** 081310(R)
[22] Hahn E L 1950 *Phys. Rev.* **80** 580
[23] Kurnita N A, Abella I D and Hartmann S R 1964 *Phys. Rev. Lett.* **13** 567
[24] Empedocles S A, Norris D J and Bawendi M G 1996 *Phys. Rev. Lett.* **77** 3873
[25] Türck V, Rodt S, Stier O, Heitz R, Engelhardt R, Pohl U W, Bimberg D and Steingrüber R 2000 *Phys. Rev.* B
     61 9944
[26] Marsal L, Besombes L, Tinjod F, Kheng K, Wasiela A, Gilles B, Rouvière J-L and Mariette H 2002 *J. Appl.
     Phys.* **91** 4936
[27] Patton B, Langbein W and Woggon U 2003 *Phys. Rev.* B **68** 125316
[28] Kuribayashi R, Inoue K, Sakoda K, Tsekhomskii V A and Baranov A V 1998 *Phys. Rev.* B **57** R15084
[29] Savona V and Parascandolo G 2007 unpublished
[30] Danckwerts J, Ahn K J, Förstner J and Knorr A 2006 *Phys. Rev.* B **73** 165318
[31] Langbein W and Hvam J M 2000 *Phys. Rev.* B **61** 1692